UCRL-TR-204727

Homopolar Gun for Pulsed Spheromak Fusion Reactors II

T.K. Fowler

June 2004

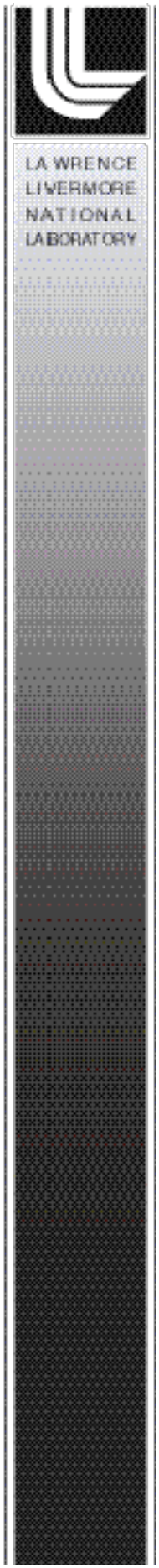

Auspices Statement

This work was performed under the auspices of the U.S. Department of Energy by University of California, Lawrence Livermore National Laboratory under Contract W-7405-Eng-48.

Homopolar Gun for Pulsed Spheromak Fusion Reactors II*

T. K. Fowler

April 23, 2004

*Revised version of paper by same title, UCRL-ID-151224, Jan. 17, 2003

Abstract

A homopolar gun is discussed that could produce the high currents required for pulsed spheromak fusion reactors even with unit current amplification and open field lines during injection, possible because close coupling between the gun and flux conserver reduces gun losses to acceptable levels. Example parameters are given for a gun compatible with low cost pulsed reactors and for experiments to develop the concept.

1. Introduction

Spheromaks are potentially attractive fusion reactors, either in steady state [1, 2] or pulsed [3,4]. Good energy confinement has been demonstrated in nearly sustained or decaying spheromaks [5], with 200 eV temperatures in SSPX even at a low magnetic field B = 0.2 T [6], and higher temperatures were achieved earlier in the CTX at 1 tesla [7]. These high temperatures presumably indicate adequate reconnection to form closed flux surfaces, at least during decay, therefore sufficient for pulsed reactors. The main issue appears to be how to build up the magnetic field efficiently, to levels required for reactors [5, 8].

Ongoing research on SSPX is investigating buildup at low gun current and high current amplification needed for a steady state reactor [5], perhaps requiring pulsing of the current to encourage intermittent reconnection during buildup [8]. High current amplification would also be attractive for pulsed reactors [4], but this may not be essential. In a pulsed reactor, energy storage must be sufficient to create the full magnetic energy of the spheromak each burn cycle. Delivering this energy rapidly via a high current gun or more slowly at low current is mainly a question of technology. In this paper, we discuss a high current gun technology based on homopolar generators.

2. Homopolar Gun Concept

The homopolar gun concept is shown schematically in Figure 1. It resembles the coaxial gun in SSPX, except that here one electrode is a rotor spinning in the bias field B_o at angular frequency ω. The spinning rotor acts as a flywheel with moment of inertia I_M, storing energy:

$$E_{ROTOR} = 1/2\, I_M \omega^2 \quad (1)$$

Because of the presence of the bias field, the spinning rotor also acts as a Faraday generator with internal radial electric field $E_r = r\omega B_o$ producing a voltage:

$$V = \int_b^a dr\, r\omega B_o = \omega(\Psi/2\pi) \quad (2)$$

where $\Psi = \int_b^a 2\pi r dr\, B_o$ is the useful bias flux across the radial gap, a - b, where current enters and exits the rotor (see Fig. 1). This voltage serves the same role as the capacitor bank usually driving current in a coaxial gun. Indeed, once current I is flowing, the rotor behaves like a capacitor, as can be seen by equating $dE_{ROTOR}/dt = - IV$, using Eq. (2) to express ω in terms of V and dividing by V to obtain [9]:

$$dV/dt = - I/C \quad (3)$$

$$C = I_M/(\Psi/2\pi)^2 \quad (4)$$

To create a spheromak using the homopolar gun, one would first spin up the rotor and then inject gas to create a plasma. After breakdown, current begins to flow around the path indicated in Figure 1, entering the rotor near the axis (if $E_r > 0$) and exiting at the rim where it returns to a stationary electrode that closes the current path. It may or may not be necessary to define this path by insulating the face of the rotor between the entry and exit annuli, since this path minimizes the resistance as we shall see. It is essential that the other electrode be stationary relative to the rotor, as must the "brushes" in a usual Faraday generator. Here the plasma replaces the brushes.

Build up of the current can be described by:

$$L_I\, dI/dt = V - IR_\omega \quad (5)$$

where L_I is the plasma inductance and R_ω is its resistance. We neglect energy in inductive acceleration of the plasma, valid for buildup slower than Alfven times, and we also omit energy in small electrostatic ExB drifts present with any coaxial gun, and viscous drag on the plasma by the rotor, specific to the homopolar gun but also small ($\omega_v < \omega_a$).

A spheromak is formed in the usual way. As I increases, the poloidal current loop shown in Figure 1 begins to expand by interaction with its own toroidal field, into the flux

conserver since it cannot expand into the solid electrodes. The poloidal bias field opposes this expansion, by inducing toroidal currents in the expanding plasma. When the gun current is large enough, expansion proceeds in any case, the induced toroidal currents serving to stretch the poloidal bias flux as the plasma expands. The threshold to do this is known as “bubbleburst”, occurring when:

$$I > I_o \equiv (\mu_o \Psi_{GUN}/\pi_o) \quad \text{bubbleburst} \quad (6)$$

where $\Psi_{GUN} = \pi b^2 B_o$ is the bias fraction injecting helicity and $\pi_o = 5/R$ with flux conserver radius R. The criterion of Eq. (6), essential to create a spheromak, is just the condition that, in expanding, the gun current I carries into the flux conserver enough helicity to create a spheromak with toroidal current $I_{TOR} = I$ [8].

We conclude that, in principle, a homopolar gun operates like any magnetized coaxial gun with the important advantage that the external power circuit is collapsed into the spinning rotor mounted directly on the flux conserver. Moreover, using advanced flywheel technology [10], the rotor can store many MJ of energy in a rotor of small size. It is this combination of close coupling of the gun and flux conserver and a large energy storage capacity that allows a homopolar gun to build up the high currents required for pulsed spheromak reactors with unit current amplification.

3. Voltage Requirements

Eq. (5) describes the buildup of current flowing along open field lines connected to the gun. As the line length L stretches at the onset of bubbleburst, L_I increases from that in the gun $\mu \pi_o a$ to include that in the flux conserver of radius R:

$$L_I \approx 1/4\, \pi_o (a + R) \approx 1/2\, \pi_o R \quad \text{after bubbleburst} \quad (7)$$

The resistance is given by:

$$IR_\pi = V_S + \pi jL \quad (8)$$

$$V_S = \pi T_e \quad (9)$$

$$j = I/A \quad (10)$$

Here V_S is the sheath voltage proportional to the electron temperature T_e in eV units; η is the plasma classical resistivity = $\eta_o / T_e^{3/2}$ with $\eta_o = 1.3 \times 10^{-3}$; and j is the current density on open lines with cross-sectional area A. Here we have omitted the rotor and electrode resistances, discussed in Section 4 and the Appendix.

Since heat conduction is fast along open field lines, we assume quasi-steady heat flow, giving for short mean-free-path:

$$\nabla j^2 = - n \chi_{||} \nabla^2 T_e \qquad (11)$$

where $\chi_{||} = (T/\eta ne^2)$. The solution to Eq. (11) is [11]:

$$T_e = 0.4 \eta j L \qquad (12)$$

with line length L. Using $\eta = \eta_o / T_e^{3/2}$ and Eq. (10), we obtain:

$$T_e = \Gamma (I/R)^{2/5} \qquad (13)$$

$$\Gamma = (0.4 \eta_o LR/A)^{2/5} \qquad (14)$$

Combining Eqs. (8), (9), (10), (12) and (13) gives the sheath and ohmic resistance:

$$R_\eta = \eta(\Gamma + 2.5) (I^{3/5}R^{2/5})^{-1} = 1.1 (I^{3/5}R^{2/5})^{-1} \qquad (15)$$

In the second step, we assume open lines filling the flux conserver at the onset of bubbleburst, giving $L \approx \pi R$ (one turn) and $A \approx 1/4 \pi R^2$ from which $\eta = 0.11$, and we take $\Gamma = 7$ that gives a best fit to SSPX data [12]. Then the minimum requirement to build up current to the bubleburst condition $I = I_o$ is, by Eq. (5):

$$V > IR_\eta = 1.1 (I_o /R)^{2/5} \quad \text{bubbleburst} \qquad (16)$$

Eq. (16) accounts for both sheath loss and ohmic resistance, the sheath loss being greater (contributing 70% for $\Gamma = 7$) but the combined losses are small nonetheless ($R_\eta \approx 40\eta\Omega$ for the reactor example below). For this Γ, at steady state T_e can also be written as:

$$T_e = 0.1 V \quad \text{steady state} \qquad (17)$$

which follows from Eq. (12) with $\Delta jL = V - V_S$ when $dI/dt = 0$. It is this increase of temperature with voltage that favors the current path in Figure 1, being the path that maximizes the voltage driving current and hence maximizing T_e and minimizing resistance.

Eq. (16) is the minimum requirement on gun voltage to create a spheromak, applicable both to fast buildup with open field lines during buildup and to slow buildup via a flux core, distinguished by:

$$I = I_{TOR} \geq I_o \quad \text{fast, open lines} \qquad (18)$$

$$I_{TOR} > I \gg I_o \quad \text{slow, flux core} \qquad (19)$$

$$B_{POL} = (\mu_o I_{TOR}/\pi R) \qquad (20)$$

where again I_{TOR} is the spheromak current giving a poloidal field given by Eq. (20) and total magnetic energy (about 2 x poloidal):

$$E_{MAG} \approx 2 \times (1/4\ \pi^2 R^3)(B_{POL}^2/2\mu_o) = 1/2\ L_I\ I_{TOR}^2 \qquad (21)$$

giving $L_I \approx 1/2\ \mu_o R$ as in Eq. (7).

For the fast method of most interest here, Eq. (16) is the design criterion, since reaching bubbleburst is tantamount to reaching the desired field level if always $I_{TOR} = I \gg I_o$ as in Eq. (18). Eq. (16) is also the design criterion for the slow method to build up $I_{TOR} >> I$ (gun) if I_o is replaced by I_{TOR} in the formula, giving:

$$V > 1.1\ (I_{TOR}/R)^{2/5} = 400\ B^{2/5} \quad \text{slow} \qquad (22)$$

Eq. (22) is obtained by calculating the channel area A for a flux core attached to the gun and threading through a closed spheromak. As B grows the spheromak field compresses the flux core, giving $A = \pi_{GUN}/B \mu\ I_o/I_{TOR}$ [8] and $LR/A = 5(I_{TOR}/I_o)$ that serves to replace I_o by I_{TOR} in Eq. (16) with about the same numerical coefficient. Helicity transport out of the flux core would introduce an additional impedance causing I to hover somewhat above I_o [8], but the main effect is that of Eq. (22) requiring a higher voltage as B compresses the flux core. Let us hold B fixed at the maximum allowed by stress levels, usually advantageous. Then,

given a voltage V exceeding V_1 needed for bubbleburst by Eq. (16), the current amplification would be:

$$I_{TOR}/I \quad \Box \quad I_{TOR}/I_o = (V/V_1)^{3/2} \quad \text{slow, flux core} \quad (23)$$

We note that, for homopolar guns, "fast" and "slow" modes are both fast. Another way to express the bubbleburst criterion is to note that resistance determines the slowest buildup time, given sufficient rotor mass so that the energy supply time $\Box (L_I C)^{1/2}$ is not limiting. For an actual buildup time $\Box \leq \Box_\Box = L_I/R_\Box$, the bubbleburst condition is $I = (V\Box/L_I) > I_o$, which gives:

$$(\Box\Box/2\Box) > (L_I\,\Box_o/\Box_o) = 5/2 \quad (24)$$

That is, with or without current amplification, achieving bubbleburst requires extracting an energy equal to that of the field at bubbleburst in about two rotation times. For $\Box \leq \Box_\Box$, Eq. (24) is equivalent to Eq. (16).

As a corollary to Eq. (24), we can estimate the injection efficiency f_{PLASMA} for the fast mode ($I = I_o$) as:

$$f_{PLASMA} = (1/2\, L_I\, I^2/IV\Box) = 1/2 \quad \text{fast} \quad (25)$$

We note also that, for pulsed reactors, V_1 to achieve bubbleburst is so large that there is little room for improvement by current amplification due to technological limits on the voltage that can be achieved in a homopolar gun. On the other hand, the current demands are so high that the homopolar gun may be the unique solution in the absence of current amplification.

Current amplification by helicity transport out of a flux core would require intermittent instability that opens and reconnects field lines [8]. An open question is whether reconnection ever occurs while the gun is on. Computer simulations [13] indicate that, though the mean field in the simulation looks like a spheromak, with constant gun voltage all of the field lines actually remain open and attached to the gun, consistent with unit current amplification observed in many experiments [5, 8]. Hereafter we will assume unit amplification and open field lines, as representative of the worst case most demanding on homopolar gun technology.

4. Example Parameters for Pulsed Spheromak Reactors

In this section, we will apply the criterion of Eq. (16) to the Low Beta scenario in Refs. [3] and [4], with parameters:

B	=	27 tesla
R	=	0.6 m
I_{TOR}	=	40 MA
E_{MAG}	=	157 MJ

We choose a = 0.4 m, b/a = 1/ 2 and $L_R = 2a$, with gun radius a and inner radius b where current enters the rotor, as in Figure 1. Then $\tau_{GUN} = \tau$. Using formulas above gives for the homopolar gun parameters:

V	=	1500 volts	
B_o	=	25 tesla	($\omega = 2\Omega$)
Ω	=	1500	(15,000 RPM)
τ	=	10 ms	

where the buildup time τ is given by Eq. (24).

These results assume unit current amplification, by equating gun current $I = I_{TOR}$ as in Eq. (18). We see that unit current amplification requires a large bias field, $B_o = 25$ tesla. Even so, this lies within the range of laboratory experience, non-destructive coil tests having been carried out up to 60 tesla [14]. We assume normal coils, rather than superconducting, thus introducing ohmic losses discussed below.

We also note the high current density in the gun, for which there is some experience with plasma arcs. In any case, our design does not appear to violate fundamentals. For example, at the high density in the reactor, $n \sim 10^{22}$ m^{-3}, the gun current does not exceed the ion saturation current. Electrode cooling is probably the main issue (see Appendix).

Turning to electrical properties, the gun resistance is estimated from $R_{GUN} = \int (j/I)^2$ integrated over the rotor volume and averaged over the buildup time as current penetrates into the plasma, as discussed in Section 6, giving crudely $<\rho>/a$ divided by 2 for the time average:

$$R_{GUN} \sim (<\rho>/2a) \qquad (26)$$

where $<\rho> \sim 2\rho_{Cu}$ (50% copper) with resistivity $\rho_{Cu} \sim 3.4 \times 10^{-8}$ for hardened copper at

high temperature [15]. Then $R_{GUN} = 0.1\Omega$, giving an ohmic power $I_{GUN}^2 R_{\Omega} = 160$ MW, or an energy loss Ω 2 MJ in a buildup time Ω= 10 ms.

Thus the gun losses are very small, much less than the internal plasma losses, as they must be for efficient buildup. This is made possible only by close coupling of the homopolar gun to the flux conserver, not feasible with conventional sources supplying the large amounts of pulsed power needed to form a spheromak in the pulsed spheromak reactor.

The ohmic loss in the bias coil is greater, but also acceptable. Using coil current $I_{COIL} = aB_o/\mu_o$, length a and thickness 1/3 a and $\rho_{Cu} \Omega$ 1.7 x 10^{-8} (with cooling), we find:

$$P_{COIL} = I_{COIL}^2(\rho_{Cu}\, 6\pi/a) = 25 \text{ MW} \qquad (27)$$

or 75 MJ per cycle for the 3-second cycle assumed below. Based on these estimates, we will take the total ohmic loss in the gun and bias coil as 75 MJ per cycle.

The burn cycle for a pulsed reactor with a homopolar gun would proceed as follows. Mechanical power is supplied continuously by a Hallbach motor coupled directly to the rotor-flywheel by a shaft, the motor and shaft having such low mass and energy content that the torque on them during buildup should be minimal (or the motor could be mechanically decoupled during the buildup). The motor draws relatively low average electrical power from the grid, about 100 MW, compared to IV = 60 GW extracted during buildup.

Between buildup pulses, the motor spins up the rotor to produce a static voltage V given by Eq. (2). The DT fuel gas is injected when V becomes sufficient to drive $I > I_o$. Introducing the gas causes breakdown and plasma formation (perhaps aided by a high voltage trigger); current begins to flow; and the magnetic field of a spheromak builds up rapidly as energy is extracted from the flywheel. After buildup, magnetic reconnection disconnects the spheromak from the gun and the gun current decays, at which point the slow replacement of the flywheel energy begins again, while the plasma burns and deposits energy in a Flibe liquid wall of high heat capacity [3, 4]. After that, the Flibe is extracted to transfer the energy to a heat exchanger and power generating system, and the cycle repeats. Injecting a Flibe layer to protect the flux conserver and gun during the burn may also aid in promoting reconnection and quenching the gun current after buildup [4].

A complete burn cycle must include energy to supply the spheromak energy plus losses, including the ohmic losses in the gun and, more importantly, internal losses in the plasma. We estimate the efficiency with respect to internal losses as 50%, by Eq. (25), giving an internal loss equal to E_{MAG} = 157 MJ. We have not included explicit energy loss during reconnection, which probably occurs during the nominal buildup time and hence is

already included in the efficiency estimate of Eq. (25). Note that to accommodate the losses the peak rotation speed must be 2 x 1500 = 2100.

With these assumptions, the total stored energy including that to supply the gun ohmic loss is 2 x 157 + 2 = 316 MJ, giving an overall gun efficiency = 157/316 ≈ 50% as assumed in Ref. [4]. Other details are given in the Appendix.

5. Mechanical Stresses and Rotor Design

The dual use of the rotor as both Faraday generator and flywheel requires a material, or combination of materials, that is both strong and highly conducting. Ordinary conductors such as copper are weak mechanically. Hardened copper alloys such as Glidcop are about as strong as the best steels [15], but even this is inadequate at rotation speeds satisfying the buildup requirement, typically requiring $\Omega > 1000$ (10,000 RPM). The Post flywheel design concept in Reference [10], already reduced to practice in industry, does operate at the required rotation speeds. However, as normally constructed the Post flywheel is not a good conductor.

A solution applying Post's design principles to a rotor combining strength and good electrical conductivity is shown in Figure 2. The Post flywheel consists of loosely coupled concentric cylinders of carbon fibers or other strong fibers bonded by epoxy or other available bonding materials. Similarly, the rotor design in Figure 2 consists of concentric dish-like shells containing both the circular strong fibers of Post's flywheel and also radial sheets or filaments of a good conductor such as Glidcop, all bonded together. The dish shape accommodates conducting paths with a radial component required for voltage generation by Eq. (2), and also an axial component that allows transfer of centrifugal forces on the conductor to the strong fibers. The parallel current paths through the shells are closed through a center conductor of small radius, giving the current path of Figure 1, with current entering near the axis and exiting at the rim. Mechanical stability follows as in Reference [10].

The hoop stress due to rotation is greatest near the rim, giving:

$$T_{HOOP} \approx \rho a^2 \Omega^2 \qquad (28)$$

where ρ is the mass density of the shells, mostly due to the Glidcop. The hoop stress is taken up by the strong fibers. However, there is also a differential stress across individual

shells that could break bonding within the shell, with magnitude $\sim(dF/dr)/A \sim \rho\Delta r\omega^2$ for shell radial thickness Δ. For N shells, $\Delta = a/N$, giving a typical bond stress:

$$T_S(\text{bond}) \quad \sim \quad (1/N)(\rho a r \omega^2) \quad < \quad (1/N)T_{HOOP} \qquad (29)$$

Torque due to j x B forces extracting energy from the rotor can be similarly diluted by the shell design of Figure 2, as discussed in Section 6.

For conceptual design purposes, the composite design of Figure 2 can be represented by average quantities depending on the volume fraction of conductor, f_{Cu}:

$$\langle\rho\rangle \quad = \quad 1000[(1 - f_{Cu}) + 8.9f_{Cu}] \qquad (30)$$

$$\langle T_{HOOP}\rangle \quad = \quad (1 - f_{Cu})\, T_S\,(\text{fiber}) \qquad (31)$$

where in Eq. (30), we take $\rho = 8900$ for copper and a nominal value $\rho = 1000$ for bond and fiber, and in Eq. (31) we neglect hoop stress taken up by the conductor. For the reactor parameters of Section 4, $\langle T_{HOOP}\rangle = 250$ ksi (half fiber, $T_S = 500$ ksi in fiber), perhaps requiring $N \geq 25$ to avoid bonding failure. In some applications below, it will be found advantageous to decrease f_{Cu} even more, in order to allow larger ω by Eq. (28) while holding T_S (fiber) at safe levels.

Other constraints on f_{Cu} are the gun resistance (not usually limiting) and ohmic heating of the conductor. Ignoring conduction during the rapid buildup gives the temperature rise in the copper with volume heat capacity C = 3.3 MJ/°Km^3:

$$\Delta T\ (^oK) \quad = \quad (E_\phi/Cf_{Cu}\pi a^2 L_R) \qquad (32)$$

During a buildup time $\tau = (5\pi/2\omega)$ by Eq. ((24):

$$E_\phi\ (\tau) \quad = \quad \int I^2 R_{GUN} \quad = \quad I^2(5\pi\rho_{Cu}/2f_{Cu}\pi a) \qquad (33)$$

with R_{GUN} from Eq. (26) and $\langle\rho\rangle = f_{Cu}^{-1}\rho_{Cu}$ and $\rho_{Cu} = 3.4 \times 10^{-8}$ for hardened copper at high temperature [15].

A convenient expression to determine experimental parameters in Section 7 is obtained from Eq. (28) with average quantities in Eqs. (30) and (31), giving:

$$\Delta a \quad = \quad 83.6(T_S)^{1/2}\,[1 + 8.9 f_{Cu}(1 - f_{Cu})^{-1}]^{-1/2} \qquad (34)$$

where now T_S is the fiber hoop stress in ksi (= 1000 psi = 7 x 10^6 Pa). Introducing this into V in Eq. (2) and introducing this result into Eq. (16) with $\Delta_{GUN} = \Delta$ gives:

$$\Delta \quad \geq \quad 400\, R^{1/3}(a/R)^{5/3}\,[1 + 8.9 f_{Cu}(1 - f_{Cu})^{-1}]^{5/6}\, T_S^{-5/6} \qquad (35)$$

For the design of Figure 2, Eq. (35) gives uniquely the minimum bias flux needed to create a spheromak by homopolar gun injection, within stress tolerance T_S. Note the advantage of a small gun radius a in reducing the required bias flux. There appears to be no limit on a in principle, the bubbleburst criterion depending on the flux conserver dimension, through Δ_o, but not the gun dimension.

6. Torque Stress

In addition to rotational stresses, the homopolar rotor also experiences shear stress due to jxB forces extracting energy from the rotor. Initially these forces are concentrated at the outer radii due to the skin effect. We can calculate the rate of penetration of current by integrating Ohm's law around a current loop, giving:

$$\int dz dA\,\{-\partial A_z/\partial t + (v \times B)_z + E_S - \eta j_z\} \quad = \quad 0 \qquad (36)$$

where z denotes distance along the current path with area weighting dA to give constant current (parallel to field lines in the plasma, with $dA = B^{-1}$). Here $(v \times B)_z$ is the z-component of the rotor EMF that produces the voltage V in Eq. (2) appearing as an electrostatic polarization voltage across the rotor face, and E_s is the sheath drop over a Debye sheath thickness at the electrode.

Eq. (36) is the local equivalent of the circuit equation, Eq. (5). As in that equation, the dominant resistance is in the sheath and plasma, and after bubbleburst the dominant inductance is that of the flux conserver. Thus current penetrates through the rotor at the rate it would penetrate into the plasma alone, in a time $\tau_\eta = L_I/R_\eta$ that includes the sheath. The radius r_I of the current boundary diffuses inward as $(a - r_I)^2 = a^2(t/\tau_\eta)$, while the gun current grows on a timescale $\tau \leq \tau_\eta$ depending on the voltage. Thus:

$$r_I \quad = \quad a(1 - (t/\tau_\eta)^{1/2}) \qquad (37)$$

$$I(t) = (t/\tau)I \geq (t/\tau_\mu)I \qquad (38)$$

where I is the final value. This tendency of the current to concentrate outward also makes the current path in Figure 1 a preferred one from the outset.

For the design of Figure 2, Eq. (37) indicates that current first builds up in the outer shell, thus applying a torque on that shell relative to inner shells. The torque T is just power divided by ω, giving:

$$T(t) = (I(t)V/\omega) = (t/\tau)(I\tau/2\pi) \leq T \equiv (I\tau/2\pi) \qquad (39)$$

Though this torque is applied in a concentrated volume, mechanical and bonding forces distribute the torque over the rotor as long as shear forces are weak enough so that the rotor acts as a rigid body. Thus, we can obtain an estimate of shear stress by assuming a rigid body, calculating the differential stress across a shell, and requiring that this not exceed the shear strength of the bonding and coupling materials. And since the total torque is greatest at the final current by Eq. (39), so also is the differential stress, allowing us to calculate only the final stresses to design the rotor.

The shear stress across one of N shells of thickness $\Delta = a/N$ is obtained by calculating the difference in torque force across the shell divided by the area of the shell. The torque acting at the surface of a shell of radius r is proportional to $(r/a)^4$, giving the following azimuthal torque force $F_\theta = T/r$:

$$F_\theta(r) = (r/a)^3(T/a) \qquad (40)$$

Then the shear stress across a shell at r is:

$$T_S(\text{shear}) = \Delta(dF/dr)/A = (1/N)(r/a)T_{SMAX} \leq (1/N)T_{SMAX} \qquad (41)$$

$$T_{SMAX} = 3(T/2\pi a^2 L_R) = (3/2\pi)(I\tau/2\pi a^2 L_R) \qquad (42)$$

where we approximate $A = 2\pi r L_R$, as if shells were cylindrical.

For the reactor example, $T_{SMAX} = 21$ ksi $<< T_{HOOP}$. Thus rotational stress is probably more important than torque shear in determining how many shells are required.

7. Parameters for Homopolar Gun Experiments

In this section, we use results of the previous sections to explore parameters for experiments to test and develop the homopolar gun concept.

a. Current Generator Experiment

The first experimental test might be a low voltage bench experiment to demonstrate the generation of current, interesting in its own right. An example setup is shown in Figure 3, in which a solid Glidcop or steel rotor at one end of a short cylinder is used to generate current to a load across a segmented stationary electrode at the other end. Parameters consistent with the strength of Glidcop (taken as 50 ksi) are:

a	=	0.2 m	
B_o	=	5 tesla	($\beta = 0.2\beta$)
β	=	1000	($\rho = 8900$, $T_S = 50$ ksi)
V	=	100 volts	

For a dead-short load, Eq. (17) gives $T_e = 0.1V = 10eV$ and $V_S = 70$ votls, giving a plasma resistivity $\eta = \eta_o/T^{3/2} = 4.1 \times 10^{-5}$ and resistance $R_\beta \approx (\eta 2a/A) = 2.6 \times 10^{-4}$ along a pathlength 2a (up and down the cylinder of length and radius a) and area $A \approx 1/2\ \pi a^2$, yielding:

I	=	$(V - V_S)/ R_\beta$	=	0.1 MA	
B	$\approx$	$(\mu_o I/2\pi a)$	=	0.8 tesla	

Higher current could be obtained by shortening the cylinder.

Experiments might include temporarily placing an insulator in front of the stationary electrode (see Figure 3). With the insulator, the plasma would polarize like the rotor and rotate with it by electrostatic ExB, but no current would flow. For experiments without the insulator, varying the load resistance would trace an I-V curve elucidating the plasma impedance properties.

b. Ringing

Before discussing spheromak experiments, we should point out a feature of homopolar guns made clear in Eqs. (3) and (5). If we neglect the losses, these equations give sinusoidally oscillating current and frequency, indicating "ringing," as would be the case for a capacitor bank with no crowbar. This is a correct physical effect, in which the jxB torque on the rotor spins up the rotor when the current reverses.

Ringing would not occur in a reactor, in which, as noted above, an incoming jet of Flibe quenches the gun current after buildup. However, ringing might occur in experiments and persist until residual magnetic energy in the gun is dissipated. There is some experience in a spheromak device without a crowbar in the BCTX experiment at U. C. Berkeley [16].

With ringing, the temperature rise would be higher than that estimated using Eq. (33) in Eq. (32), a better guess being $E_{\Delta} = 1/2\ E_{MAG}$ □ the residual magnetic energy in the gun after buildup is over.

c. Spheromak Experiments

We list below examples of experiments sufficient to produce spheromaks using the homopolar gun design of Figure 2, described by Eq.(35). Cases are labeled by their potential roles in a development program. Details are given in Tables 1 and 2.

The order of calculation employed here is first to choose dimensions a and R, conductor fraction f_{Cu} and hoop stress T_S, which determines □ by Eq. (28) and the lower bound on the bias flux □ entered in the tables by Eq. (35), from which we can calculate B and I, and so on. The temperature excursion in the conductor is obtained from Eq. (32).

Table 1 shows the result of using to advantage a varying conductor fraction f_{Cu} to obtain moderate fields and magnetic energies, scaling up to ignition and pulsed reactors in Case 5. All cases in Table 1 assume a composite rotor, like Figure 2, with T_S = 500 ksi. Note that this is stress on the carbon fibers, not the average stress (see Eq. (31)). In all cases, it is assumed that the rotor energy must be about $2E_{MAG}$ to compensate for losses. For Cases 1, 2 and 3, the rotor energy is greater than needed, the rotor length-to-radius ratio being chosen to limit the temperature excursion. Table 2 repeats Case 4 of Table 1 with a variation of the stress T_S.

For all cases, the temperature rise shown in the tables corresponds to $E_{\Delta} = 1/2\ E_{MAG}$ in Eq. (32) to account for ringing in experiments as discussed in Section 7b above. The temperature rise during buildup, with E_{Δ} in Eq. (33), is very small, < few °K for all cases. This very low resistive temperature excursion in the rotor would be correct for pulsed reactors, in which Flibe injection quenches the current after buildup.

The following are key examples, discussed below. Case numbers follow labels in the tables. Parameters listed are the rotor speed □, gun radius a, flux conserver radius R, gun voltage V and spheromak field B:

		□ (s^{-1})	a(m)	R(m)	V(volts)	B(T)
Case 1, SSPX	8950	0.2	0.5	580	2.6	

Case 4, Proof-of-Principle	2970	0.2	0.6	968		9.0	
Case 5, Ignition		1500	0.4	0.6	1500		27.0

c. Possible SSPX Experiments

Case 1 is marginally applicable to an experiment in SSPX, though the full bubbleburst current leads to a magnetic field B = 2.6 tesla that is perhaps beyond the strength limits of the existing flux conserver.

Note the small size of the gun, a = 0.2 m, needed to take advantage of the reduction factor $(a/R)^{5/3}$ in Eq. (35). However, there is no essential reason for a large gun, the bubbleburst criterion being independent of gun size, as noted above.

Note also the high rotor speed □ required to provide sufficient voltage at a bias flux low enough to allow bubbleburst at this field and current level. However, it is □a, not □, that counts in determining tensile stress.

The small conductor fraction for this case gives a higher temperature rise. The rotor length, chosen to limit the temperature excursion, gives a large rotor energy requiring a long spin up time (e.g. one minute for a 0.3 MW drive motor).

d. Proof-of-Principle Experiment

Case 4, explored further in Table 2, might be the basis for a proof-of-principle test demonstrating homopolar gun performance and spheromak energy confinement up to B = 9 tesla, sufficient to reach temperatures of many KeV after reconnection, and the confinement regime of reactors.

Note that reducing the fiber stress limit gave a rotation speed and rotor energy too small to achieve bubbleburst. For that case (Case 4a, T_S = 250 ksi), the current is obtained by equating E_{MAG} to E_{ROTOR} from Eqs. (1) and (21).

e. Ignition Experiment

Case 5 meets the estimated requirement for ohmic ignition, given approximately by $BR > 16/(\square B)^{1/3}$[3]; or, in terms of current, with □ □ 3%:

$$I(MA) > 46\, R^{1/4} \quad \text{ignition} \qquad (43)$$

Parameters for this case correspond to those of the pulsed spheromak reactor in Refs. [3] and [4], discussed in the next section. With 50-50 DT fuel, the fusion yield would be about 3GJ. Ignition may still occur with a lower fraction of tritium and lower yield. Parameters have not been optimized.

Note the larger gun dimensions for this case, needed to supply the required magnetic energy meeting the ignition condition above.

The rotor design for this case exemplifies the ability of the Post flywheel to store energy in a compact space, storing 360 MJ with rotor radius only 0.4 m and length 0.8 m (see Appendix). With moment of inertia I_M = 160 kgm^2 and bias flux Φ = 2π webers, the rotor has an equivalent capacitance by Eq. (4) of 160 Farads but a modest voltage (< 2 kV).

8. Isolating the Homopolar Generator

As shown in Figure 4, the homopolar generator plasma could be isolated from the spheromak by inserting an annular stationary electrode like that in Figure 3 between the rotor and the cylindrical electrode of Figure 2. The annular electrode, with an insulator between the rim and axis, would act as a coaxial gun fed by the rotor generator. One advantage might be flexibility in choosing a plasma of different atomic composition and density in the generator, potentially a way of handling surface heat loads on the rotor as discussed in the Appendix. While the voltage requirement would increase due to resistance on the rotor side, this could be greatly reduced and heat loads on the rotor reduced also by making the gap distance d between the rotor and annular electrode small, so as to reduce Φ in Eq. (14) for this additional resistance. Isolating the generator would also make possible higher generator voltage using the known technique of a rotor made up of several disks in series.

By lengthening the annular gun electrode structure so that generator bias flux expands in passing to the gun side, the bias at the rotor Φ_{ROT} can be greater than Φ at the gun, thereby breaking the strict requirements of Eq. (35) though Eq. (16) must still be satisfied. This is equivalent to supplying power to a conventional coaxial gun by means of an independent homopolar generator, but doing so in a compact design that eliminates the conventional busbar, the extended annular electrode itself serving as the "busbar." This approach would allow us to obtain the voltage needed to satisfy Eq. (16) by pushing the rotor bias B_{ROT} to its technological limits rather than the rotor itself. For example, taking σ_a = 200 for Glidcop (50 ksi, as in the experiment of Section 7a) and $\Phi_{ROT} = \sigma_a a^2 B_{ROT}$, the voltage that could be obtained from a Glidcop rotor is:

$$V = \omega(\Phi_{ROT}/2\pi) = 100 B_{ROT} a \quad \text{Glidcop} \qquad (44)$$

Taking a = 0.4 m as in the pulsed reactor design of Section 4 and B_{ROT} = 40 T (less than the maximum 60 T obtained in the laboratory to date without destroying the coil [14]), we

obtain V = 1600 sufficient for the reactor, with $\lambda_{ROT} = 6.4$, conveniently expanded to $\lambda = 2$ over a short annular electrode. Using conventional coils, the coil power would be prohibitive, requiring perhaps a shielded superconducting outer coil with a conventional coil inside it. Similarly, for $B_{ROT} = 10$ T and a = 0.3 m gives V = 300 volts, perhaps a suitable candidate for a small second gun in SSPX.

These ideas could be applied to a compact design like Figure 4, with a Glidcop rotor.

9. Conclusions

The homopolar gun concept described here builds on laboratory experience demonstrating good heat confinement in nearly sustained or decaying spheromaks, and it bypasses in a pulsed spheromak reactor the requirement for high current amplification that appears to be essential for a steady state reactor.

An essential feature is the close coupling of the gun and flux conserver, making possible a very low gun resistance, typically < 1 Ω by Eq. (26). Thus the gun can drive very high current at moderate voltages. Homopolar generators are inherently low voltage, high current devices well suited to this application.

The proposed buildup cycle including helicity injection and subsequent relaxation to a closed configuration with ohmic heating to ignition temperatures could be modeled on NIMROD [13].

An experimental program to develop a pulsed spheromak reactor with high current gun injection is discussed briefly in Section 7, using the design of Figure 2, and in Section 8, using the design of Figure 4. We conclude that, based on the examples of Tables 1 and 2, homopolar guns are particularly useful to achieve magnetic fields higher than those attainable in SSPX, while an extended SSPX program with more capacitor bank energy could explore the regime up to B = 1 tesla (T $\approx$ 1 keV), even with unit current amplification, in order to verify further the processes of formation, reconnection and energy confinement in spheromaks prerequisite to ignition experiments and reactors based on homopolar guns.

The immediately useful experiment would be the bench test of homopolar current generation discussed in Section 7a, yielding perhaps 0.1 MA at 100 volts with a solid Glidcop rotor of 20 cm radius spinning at 10,000 RPM. Experiments with such a device would elucidate problems and motivate design improvements.

Acknowledgements

I would like to thank many colleagues for useful comments, especially: Simon Woodruff, Harry McLean and Bruce Cohen for conversations leading to this study; Dick Post for discussions of flywheel technology and rotating rotor design; and Keith Thomassen for discussions of homopolar generators.

References

[1] R. L. Hagenson and R. A. Krakowski, Fus. Tech. **8**, 1601 (1985).

[2] R. W. Moir, R. H. Bulmer, T. K. Fowler, T. D. Rognlien and M. Z. Youssef, "Spheromak Magnetic Fusion Energy Power Plant with Thick Liquid Walls," ANS Topical Conference, Washington DC, 2002.

[3] T. K. Fowler, D. D. Hua, E. B. Hooper, R. W. Moir and L. D. Pearlstein, Comments Plas. Phys. Contr. Fusion, Comments on Mod. Phys. **1**, Part C, 83 (1999).

[4] T. K. Fowler and Per F. Peterson, "Conceptual Design of a Pulsed Spheromak Fusion Power Plant," Department of Nuclear Engineering, University of California, Berkeley, Report UC-BFE-052, November 5, 1998.

[5] D. Hill, R. H. Bulmer, B. I. Cohen, E. B. Hooper, H. S. McLean, J. Moller, L. D. Pearlstein, D. D. Ryutov, R. D. Wood, S. Woodruff, C. T. Holcomb, T. Jarboe, P. Bellan and C. Romero, International Conference on Controlled Thermonuclear Fusion, Lyon, France, October, 2002.

[6] SSPX Team, APS Division of Plasma Physics, Orlando, November, 2002.

[7] T. R. Jarboe, F. J. Wysocki, J. C. Fernandez, I. Hennins and G. J. Marklin, Phys. Fluids B **2**, 1342 (1990).

[8] T. K. Fowler, D. D. Hua and B. W. Stallard, "Spheromak Impedance and Current Amplification," UCRL-ID-147087, January 31, 2002.

[9] K. I. Thomassen, "Fusion Applications of Fast Discharging Homopolar Machines," Los Alamos Scientific Laboratory, Topical Report ER-625, Research Project 469, January, 1978.

[10] R. F. Post, T. K. Fowler and S. F. Post, Proc. IEEE **81**, 462 (1993).

[11] R. H. Cohen, E. B. Hooper and D. D. Ryutov, "Joule Heating of the Plasma on the Open Field Lines," SSPX Memo, Sept. 11-20, 2000; R. W. Moses, R. A. Gerwin and K. F. Schoenberg, Phys. Plasmas **8**, 4839 (2001).

[12] B. W. Stallard, S. Woodruff, R. H. Bulmer, D. N. Hill and E. B. Hooper, H. S. McLean, R. D. Wood and the SSPX Team, "Magnetic Helicity Balance in the SSPX Spheromak," submitted for publication in Phys. Plasmas, 2002.

[13] C. R. Sovinec, J. M. Finn and D. del- Castillo-Negrete, Phys. Plasmas **8**, 475 (2001).

[14] Reported in Science, **281**, 1262 (1998).

[15] Glidcop data, provided by OMG Americas.

[16] E. Coomer, C. W. Hartman, E. Morse and D. Reisman, Nuclear Fusion **40**, 1669 (2000).

[17] T. J. Dolan, *Fusion Research*, Pergamon Press, New York, 1982, Chap. 6, breakdown; Chap. 20, cooling pump power; Chap. 26, heat transfer.

Table 1. Homopolar Gun Parameters for Spheromak Experiments

Design Parameters

Case	a(m)	R(m)	L_R(m)	f_{Cu}	Φ(Web)	B_o(T)
1	0.2	0.5	0.2	0.01	0.41	3.3
2	0.2	0.6	0.05	0.1	0.54	4.2
3	0.2	0.6	0.1	0.25	0.96	7.6
4	0.2	0.6	0.6	0.5	2.05	16
5	0.4	0.6	0.8	0.5	6.28	14

Operating Parameters

Case	ω(s^{-1})	B(T)	I(MA)	T_S(ksi)	V(volts)	E_{MAG}(MJ)	E_{ROT}(MJ)	ΔT(°K)*
1	8950	2.6	3.3	500	580	0.83	22	500
2	6625	2.3	3.5	500	570	1.2	5	284
3	4690	4.2	6.3	500	716	3.8	8	183
4	2970	9.0	13.5	500	968	17.6	33	211
5	1500	27	40	500	1500	157	360 (peak)	216

*For $E_\Phi = 1/2\ E_{MAG}$ here and in Table 2. See text.

Table 2. Case 4, Table 1, with Variable T_S

Design Parameters

Case	a(m)	R(m)	L_R(m)	f_{Cu}	Φ(Web)	B_o(T)
4a	0.2	0.6	0.6	0.5	2.84	23
4b	0.2	0.6	0.6	0.5	2.05	16
4c	0.2	0.6	0.6	0.5	1.46	12

Operating Parameters

Case	Γ(s^{-1})	B(T)	I(MA)	T_S(ksi)	V(volts)	E_{MAG}(MJ)	E_{ROT}(MJ)	ΔT(°K)*
4a	2100	8.8	13.2	250	948	16.5**	16.5	199
4b	2970	9.0	13.6	500	968	17.6	33	211
4c	3635	6.5	9.73	750	845	9.01	49	217

**Limited by $E_{MAG} = E_{ROT}$; no bubbleburst. All other cases satisfy Eq. (35).

Appendix. Pulsed Spheromak Fusion Reactor

In this Appendix, we give more details for the reactor discussed in Section 4. In that section, ohmic losses in the gun and bias coil were estimated as 75 MJ per burn cycle. To avoid sputtering and for other reasons discussed below, it may be necessary to clad Glidcop surfaces exposed to the plasma with tungsten, but this would not significantly affect resistance. As was also discussed in Section 4, in addition to ohmic losses, the flywheel must provide 157 MJ of magnetic energy to the spheromak and an estimated additional 157 MJ to account for internal losses in the plasma.

Combining these estimates with those of Ref.[4] gives the following energy budget for a burn cycle:

Thermal output from fusion yield	3768 MJ
Electric output (40% conversion efficiency)	1507 MJ
Input to spheromak field	157 MJ
Plasma internal losses and residual energy in gun	157 MJ
Gun and bias coil losses	75 MJ
Net to customer	1118 MJ
Plant efficiency = 1118/3768	30%

We have omitted allowance for heat transfer and auxiliaries, perhaps reasonable given the simplicity of the system. Estimates indicate that heat loss associated with transferring Flibe from the reactor chamber to the heat exchanger could be only 1 MJ per cycle.

The homopolar generator rotor for this case is that in Case 5, Table 1, with radius a = 0.4m and length L_R = 0.8m and average density <□> = 5000 (50% Glidcop), giving a rotor mass M = 2000 kg and moment of inertia I_M = 160 kgm^2. At the peak rotor speed □ = 2 x 1500, Eq. (1) gives a stored energy exceeding buildup requirements of 316 MJ:

E_{ROTOR} = 1/2 I_M□^{2} = 360 MJ peak

The rotor mass and that of the Hallbach motor are small compared with 100 tons for the reactor chamber [4]. Hence the reactor cost is unchanged, nominally $15 M for the heat source [4]. We assume a cycle time of 3 seconds, giving:

Cycle period	3 sec
Net Power out = 1118/3	370 Mwe

This gives a nominal capital cost of $40/KWe for the reactor chamber and gun assembly. The overall plant efficiency is 30% for the numbers above.

Other features and issues discussed in Ref. [4] are similar. The gun and bias coils (□ 3 tons) might triple the copper waste stream, still only 4 tons/year including the flux conserver. Despite the close coupling of the gun to the reactor chamber, the protective Flibe layer would tend to flood the gun during the burn, thereby shielding the gun, and copper alloys continue to harden under radiation [15]. These alloys also swell under radiation [15]. We do not yet have information on neutron damage to other rotor materials.

Another important issue is surface heating of electrodes by sheath and plasma losses [12]. These losses (157 MJ) greatly exceed the electrode surface heating capacity, ultimately requiring absorption in Flibe to become part of the overall heat load extracted by Flibe coolant each burn cycle. A precursor injection of about 20 kg of Flibe is needed.

One approach to handling surface heating would be to isolate the rotor from the flux conserver using the design concept of Figure 4, mentioned in Section 8, in which an annular electrode like that in Figure 3 is inserted between the rotor and flux conserver. Using formulas in Reference [17], we estimate that a spacing d = 2.5 mm gives a time-averaged resistive heat load of 1.1 GW, using □ in Eq. (14) for this d, depositing 11 MJ on the rotor and electrode surfaces during a buildup time □= 10 ms. (Increasing the spacing to d = 1 cm increases the deposition to 19 MJ.) Thin tungsten cladding □ 1 mm thick, bonded to the inner surface of the dish rotor (where carbon fiber can take up centrifugal force stress), and

also on the annular electrode, can absorb this energy without cooling (hemispheric shape giving $A = 2\pi a^2 = 1 m^2$ rotor surface area, thermal conductivity K = 163, mass heat capacity C = 134, density ρ = 19,300 in MKS units, giving ΔT = 3000 °K below the melting point = 3370 °K). Helium gas can carry this heat away between burn cycles, the helium serving also as the gas to create the plasma "brushes" between the rotor and annular electrode. By routing helium through perforations in the rotor shaft, the rotor itself can pump the helium with a pumping speed $\propto$ p_{He}, giving a cooling power $\propto$ 80 p_{He} in MW with helium pressure p_{He} in ksi. Steady cooling at an average rate 3.7 MW would suffice, giving p_{He} = 0.05 and a product $n_{He}d = 2 \times 10^{22}$ near the minimum of the Paschen breakdown curve (and an electron mean free path << d, consistent with our equations). A pressure burst p_{He} = 12 ksi (requiring a plenum and valve) could provide active cooling matching the 1.1 GW heat deposition rate during buildup, probably requiring a voltage spike for breakdown.

A precursor 20 kg of Flibe would still be required to protect the annular electrode on the side facing the flux conserver. Injection over the 10 ms buildup, at velocity $v = a/\tau$ = 40 m/s, requires little energy but does add resistance across the Flibe layer, around 15 $\mu\Omega$ for a layer thickness 3 mm, compared to $R_\square$ = 37.5 $\mu\Omega$ by Eq. (16). Adding to this the 2.5 $\mu\Omega$-equivalent resistance depositing 11 MJ in the rotor chamber, we require a voltage increase of 17.5/37.5 = 46%, to V = 2.2 kV. This voltage increase could be accommodated by a reduction in conductor fraction to f_{Cu} = 26% allowing a 47% increase in rotation frequency at the same fiber stress. At the higher ω,the same rotor length 0.8m would provide the additional rotor energy required. The rotor/electrode internal resistance would only increase to 0.2 $\mu\Omega$. The injected Flibe would also produce gaseous vapor which might contribute to energy absorption and dispersion as radiation, as in a "gaseous divertor."

Finally, we note that, while we have spoken of a separate Hallbach motor to drive the rotor, as indicated in Figure 4 it is possible that electric power can be supplied directly to spin up the rotor acting as a motor. A 120 MW d.c. power supply with voltage > 3 kV (the rotor voltage at peak charge) would suffice. Applying the power requires brushes at the rotor axis and rim, and it is probably this (and rotor insulation) that determines the desirable voltage to reduce the current to that which the brushes can handle. The cost of this 120 MW power supply, of conventional solid state design, would probably exceed other costs mentioned above. The d.c. power could be provided continuously to drive the rotor as a pump and to slowly recharge the rotor between burn cycles, the overall system acting as an intermittent load (the spheromak) with a capacitor (the rotor) across the load. As described in Section 4, the current would be initiated by injection of DT gas in the flux conserver and extinguished by a thick Flibe layer injected when burn commences in order to protect the

flux conserver and gun from neutron damage. The Flibe layer, about 10 cm thick, introduces a much higher resistance giving a decay time L/R ≈ 25 μs for the gun current after reconnection. This decay energy has already been accounted for in the 157 MJ of internal losses in the table above.

The increase in losses to accomplish cooling by the approach described above [about 1 (rotor/electrode) + 11 (rotor plasma brush) + 63(Flibe) = 75 MJ total] is offset by recovering thermal energy in the Flibe for which credit has not been taken, now totaling 63 + 2 x 157 = 377 MJ per cycle. This gives a new energy balance, as follows:

Thermal output from fusion yield	3768 MJ
Thermal recovery	377 MJ
Total thermal input to generators	4145 MJ
Electric output (40% conversion efficiency)	1658 MJ
Losses accounted for above (314 MJ recoverable)	389 MJ
Surface cooling losses (63 MJ recoverable)	75 MJ
Net to customer	1194 MJ
Plant efficiency = 1194/4145	30%

Thus the overall performance is about the same.

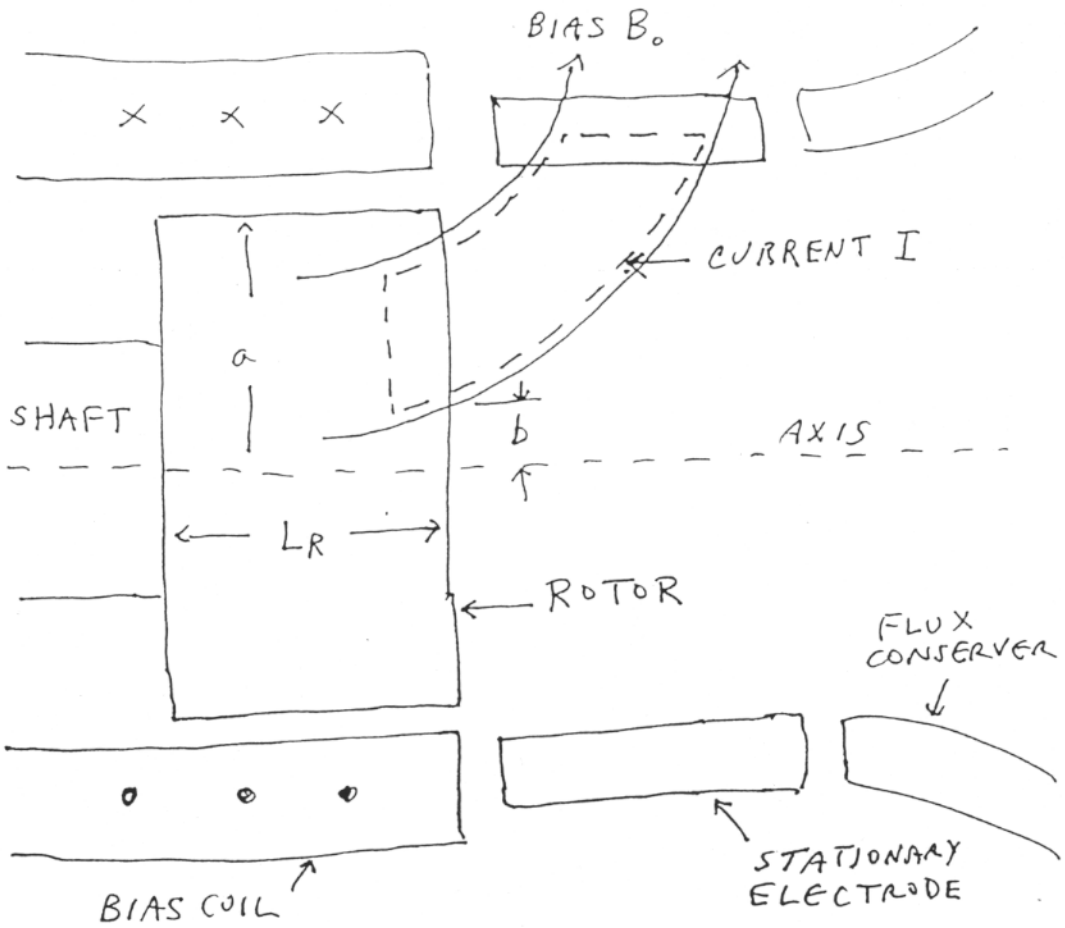

Figure 1. Schematic design of homopolar gun.

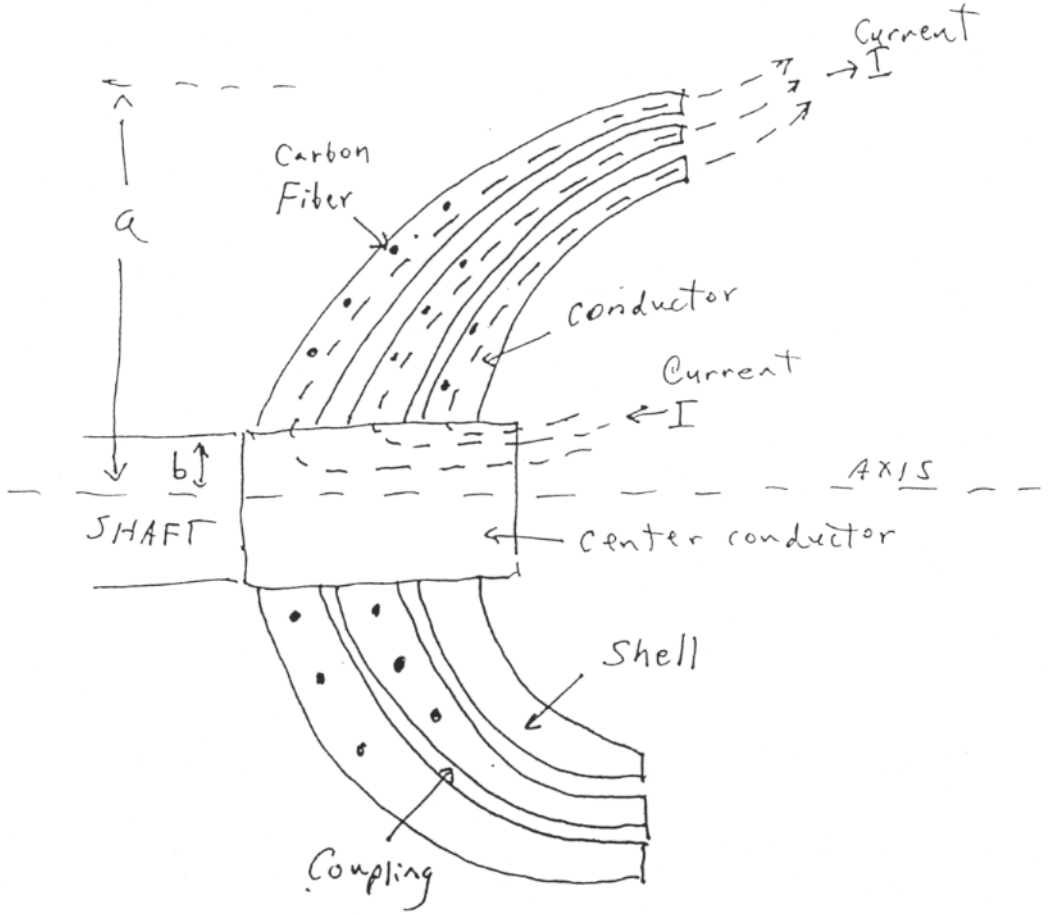

Figure 2. Composite rotor design consisting of concentric dish-shaped shells made of ciranlar carbon rings embedded in conductor.

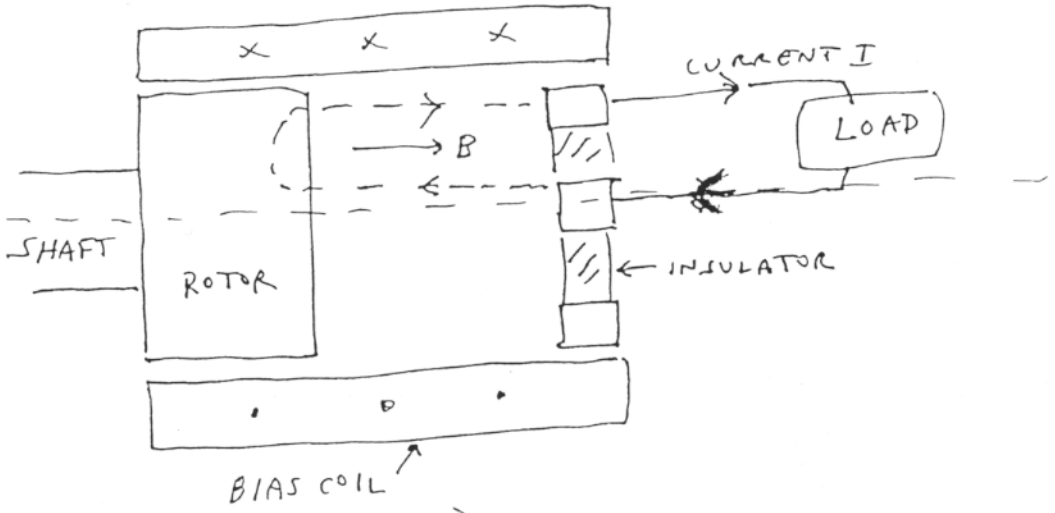

(A)

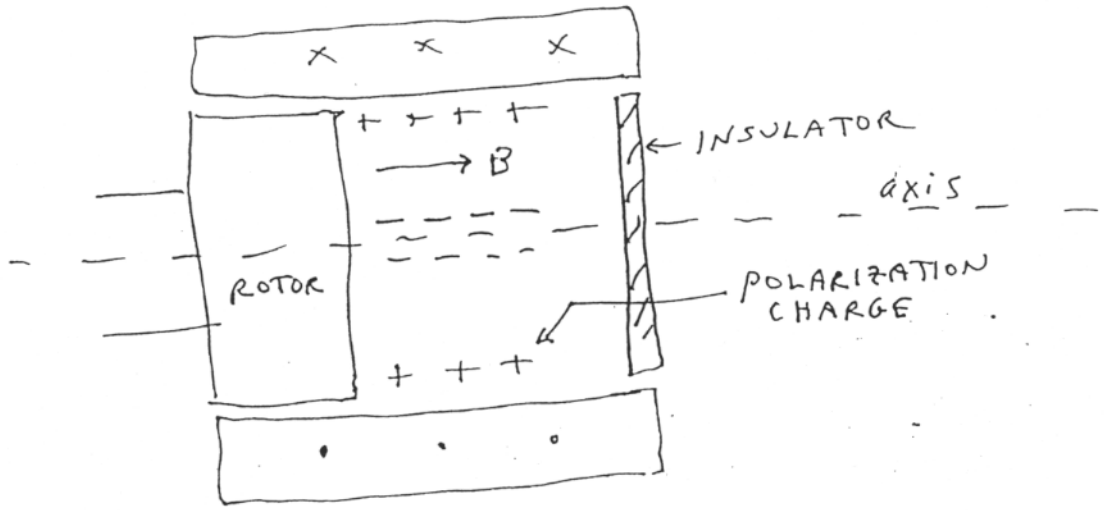

(B)

Figure 3. Current generator experiment, with (A) variable load and (B) temporary insulator to prevent closure of current loop.

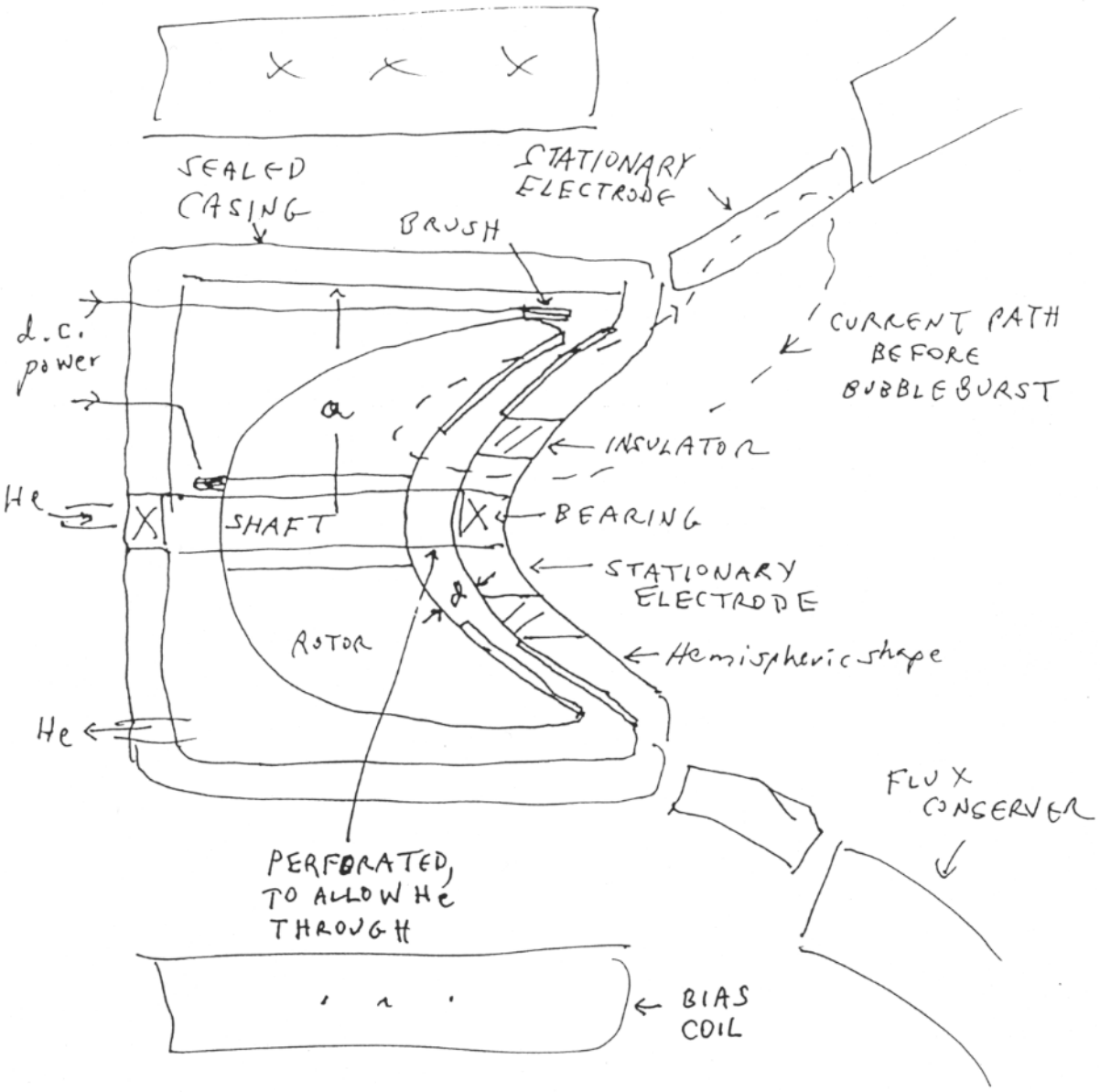

Figure 4. Isolated Rotor Schematic Design